Journal of Molecular Structure 1114 (2016) 197–205

Contents lists available at ScienceDirect

Journal of Molecular Structure

journal homepage: http://www.elsevier.com/locate/molstruc

Probing the adsorption and orientation of 2,3-dichloro-5,8-dimethoxy-1,4-naphthoquinone on gold nano-rods: A SERS and XPS study

Maraizu Ukaegbu [a], Nkechi Enwerem [a], Oladapo Bakare [a], Vichetra Sam [b], William Southerland [b], Alberto Vivoni [c], Charles Hosten [a, *]

[a] Howard University, Department of Chemistry, 525 College Street NW, Howard, Washington, D.C. 20059, USA
[b] Research Centers in Minority Institution, School of Medicine, Howard University, Washington, D.C. 20059, USA
[c] Department of Biology, Chemistry and Environmental Sciences, Inter American University, San German, PR 00683-9801, USA

ARTICLE INFO

Article history:
Received 3 February 2015
Received in revised form
9 February 2016
Accepted 10 February 2016
Available online 11 February 2016

Keywords:
Surface-enhanced Raman (SERS)
Density functional theory (DFT)
Adsorbate orientation

ABSTRACT

2, 3-Dichloro-5,8-dimethoxy-1,4-naphthoquinone (DDNQ) is a synthetic naphthaquinone which has shown reduced chemotoxicity and enhanced chemotherapeutic activity in *in vitro* studies. The ability of DDNQ to serve as a chemical dopant of graphene resulting improved performance of graphene by tuning its band gap is also being explored. In this report surface enhanced Raman scattering (SERS) spectroscopy was utilized to probe the adsorption/orientation of DDNQ on gold nano-rods. Interpretation of the SERS data required a complete assignment of the vibrational modes of DDNQ and this was performed with DFT calculations using BP86/6-31G (d, p), B3LYP/6-31G (d) basis sets, and potential energy distribution (PED) calculations. Surface selection rules and relative band enhancement factors were utilized to propose an orientation and mode of interaction for DDNQ adsorbed on Au nanosurfaces. XPS data supported the conclusions obtained from the SERS data.

1. Introduction

Metal nanoparticles have attracted interest in recent years due to their potential application in the fields of sensing [1,2], photonic [3,4], and biomedicine [5,6]. Because of their unique properties, tunable sizes, biocompatibility, and surfaces capable of chemical modification, gold and silver nanoparticles have been exploited as drug delivery devices and nanosensors [7,8]. These functionalized nanoparticles offer the potential to improve drug transport and action, as well as significantly reducing the therapeutic dosage thereby minimizing the side effects of the drugs. While both gold and silver nanoparticles have been used as drug delivery systems gold has the advantage of biocompatibility, ease of surface modification, and a significant degree of cell penetration [9]. Cheng and coworkers have shown that 5 nm Au nanoparticles coated with polyethylene glycol can serve as a delivery system for use in photodynamic therapy of cancer [10]. Dreaden, using Tamoxifepoly(ethylene glycol)-thio gold nanoparticles, has established that this modified nanoparticle can serve as a highly selective delivery system for breast cancer treatment with the drug exhibiting enhanced potency [11]. In this study the authors also established that the nanoparticle drug delivery systems exhibited selective intracellular delivery of the tamoxifen-targeted gold nanoparticles to the specific breast cancer cell lines.

Because of its high molecular specificity Raman spectroscopy can selectively identify molecules based on their unique spectral signatures. The application of Raman spectroscopy, however, is limited by the inherent low intensity of the Raman scattering. It has been shown that the Raman scattering efficiency can be increased by up to six orders of magnitude if the analyte is situated on the surface of a noble metal (Ag or Au). This amplification of the Raman signal (Surface-Enhanced Raman Scattering) has found application in the tracking of drug delivery systems in single cells. Zong fabricated a carrier system consisting of a core shell system with the Raman molecule tagged AU@Ag nanorods (SERS active core) and mesoporous silica as the drug containing shell which delivered the anticancer drug doxorubicin. The authors were able to track the location of the nanocarriers by SERS [12].

As biofunctionilization of nanoparticles increases it is ever more important to identify the functional groups which are involved in

* Corresponding author. Howard University, Department of Chemistry, 525 College St. NW, Washington, D.C. 20059, USA.
E-mail address: chosten@howard.edu (C. Hosten).

http://dx.doi.org/10.1016/j.molstruc.2016.02.043
0022-2860/

binding to the metal surface, the nature of the interaction, and any structural changes to the biomolecules which might occur as a result of their binding to the metal surface. These interactions can affect both the bioactivity and bioavailability of the molecules once they are attached to the metal surface [13]. In this report the adsorption characteristics of 2, 3-Dichloro-5,8-dimethoxy-1,4-naphthoquinone (DDNQ) on Au nanoparticles are reported. The mode of interaction between DDNQ and the coinage metal surface was determined, and SERS surface selection rules allowed for the determination of the orientation of adsorbed DDNQ relative to the surface normal.

2. Experimental section

2.1. Chemicals

Analytical grade silver nitrate ($AgNO_3$), sodium borohydride ($NaBH_4$), gold (III) chloride trihydrate ($HAuCl_4.3H_2O$), hexadecyltrimethylammonium bromide (CTAB), ascorbic acid, cyclohexane, and absolute ethanol were purchased from Sigma–Aldrich and used as received. Singly distilled deionized water was used for the preparation of the gold nano-rods.

2.2. Synthesis

2, 3-dichloro-5, 8-dimethoxy-1, 4-naphthoquinone was synthesized as described by Copeland and Huang [14,15].

2.3. Synthesis

Gold nano-rods were synthesized by a slight modification of the methods reported by Murphy [16] and Primera-Pedrozo [17]. The synthesis involves two steps (A and B):

2.3.1. Seed preparation

250 μL of an aqueous solution 0.01 M of $HAuCl_4.3H_2O$ were added to 7.5 mL of 0.1 M CTAB solution in a 50 mL plastic centrifuge tube. After gentle mixing, 600 μL of chilled 0.01M $NaBH_4$ solution were added. The solution was stirred for 3 min during which time it turned a pale-brown yellow color. This solution was left undisturbed for 2 h at 25 °C.

2.3.2. Gold nano-rods preparation

1.8 mL of 0.01 M $HAuCl_4.3H_2O$ solution and 270 μL of 0.01 M $AgNO_3$ solution were added to a 42.75 mL 0.1 M CTAB solution in a 50 mL plastic centrifuge tube. The resulting solution was gently mixed, followed by the addition of 0.1 M aqueous ascorbic acid solution (288 μL). After the solution became colorless, 90 μL of the seed solution were added to the mixture and the reaction tube was allowed to sit undisturbed for 3 h at 30 °C during which time the solution developed a blue color. The resulting solution, containing the gold nano rods, was concentrated and separated from the excess surfactant by washing and centrifugation (the microtubes were centrifuged at 14,000 rpm for 15 min). The supernatant was carefully removed from each microtube, deionized water was then added to the microtube, and the resulting solution was centrifuged. This process was repeated two times. At the completion of the centrifugation process UV–visible spectra were recorded by diluting 250 μL of the solution containing the gold nano rods with deionized water to a final volume of 0.50 mL.

2.4. Deposition of gold nano rods on silicon wafer (SERS substrates)

The gold nano rods were deposited onto the silicon wafer using a modified form of the procedure developed by Primera-Pedrozo [17]. 2 mL of the gold nanorods solution were mixed with 3 mL of deionized water and transferred to a glass beaker. Two mL of cyclohexane were added to the gold nanorods solution and an immiscible water/cyclohexane interface was formed. This was followed by the dropwise addition of 2 mL of absolute ethanol which resulted in the formation of a film of gold nano-rods at the cyclohexane/water interface. Ethanol facilitates the remove of the remaining surfactant and also acts as an inducer [18,19]. The bottom cyclohexane phase was slowly removed until the silicon wafer was randomly covered with Au nanorods. The morphology of the gold nano rods on the silicon wafer was determined using Scanning Electron Microscope (SEM). DDNQ was then adsorbed onto the Au nanorods from a 10^{-3} M DDNQ solution.

2.5. Methods

The UV–visible absorption measurements were carried out with a Hewlett Packard 8453 UV–Visible spectrophotometer. The infrared spectra were recorded with a PerkinElmer Spectrometer. Surface-enhanced Raman scattering (SERS) spectra were recorded using a DeltaNU MicroRaman Microscope having 633 and 532 nm laser lines and a laser power of less <2 mW.

2.6. XPS measurements

The gold (III) substrate, having a thickness of 200 nm was purchased from PHASIS Company. SAMs of DDNQ molecules on the gold surfaces were formed by immersing the gold substrate in 1 mM DDNQ solution for 24 h at 30 °C. After the modification, the gold surface was rinsed with methanol and dried under N_2. The XPS spectra were acquired using a Kratos Axis 165 spectrometer equipped with a monochromatic A1 radiation source. The sample was deposited on the sample holder which was kept at about 25 °C. The pressure of the spectrometer was maintained at 5×10^{-8} Torr and the take-off angles were 0°, 50° and 70° with respect to surface normal. The instrument was calibrated using sputter cleaned high purity copper and gold foils. The peak positions were calibrated to the hydrocarbon peak at 284.8 eV present on the surface of the sample.

2.7. Theoretical calculations

The Gaussian 98W program was used for all Quantum Mechanical Computations. The full geometry optimization and vibration frequency calculations were performed using BP86/6-31G (d, p), B3LYP/6-31G (d) basis sets. The assignment of the experimental frequencies was based on matching the observed and calculated band frequencies, calculation of the percentage difference between the frequencies of the observed and calculated Raman spectra, and comparison with literature data. PED calculations were performed to aid the assignment of the vibration modes [20].

3. Results and discussions

A prerequisite for determining the preferred adsorption characteristics of DDNQ adsorbed on the metallic nano-surface was the assignment of the Raman active modes of DDNQ.

3.1. Band assignment of vibrational spectra

DDNQ has 26 atoms and C2v symmetry. Under C2v symmetry the 72 fundamentals of DDNQ are distributed among the symmetry elements as;

$$\Gamma vib_{(3N-6)} = 24A1 + 23B2 + 13A2 + 12B1$$

with the A1 and B2 irreducible representations corresponding to stretching, in-plane ring deformation, and in-plane bending vibrations, while the A2, B1 correspond to out of plane ring deformation, torsion, and out of plane bending vibrations. A complete vibrational assignment of the observed DDNQ frequencies was performed based on the results of a normal mode analysis, frequency matching of theoretical and experimental frequencies, and the data obtained from the PED calculations. Two main factors are responsible for the reported differences between the observed and the calculated frequencies of DDNQ: (i) the calculated frequencies of DDNQ are performed in an isolated environment, and (ii), the experimental frequencies are inharmonic frequencies while the calculated frequencies (or values) are harmonic frequencies [21]. The percentage differences between the observed and the calculated frequencies ranged from a low value of 0.06 to a high of 3.37.

The BP86/6-31G (d, p) and B3LYP/6-31G (d) basis sets were used for the DFT calculation. The B3LYP/6-31 (d) basis set has been shown to over-estimate the frequencies in the high frequency region and as a result a scaling factor was applied. The scaling factor was determined based on the ratio of the experimental frequencies to the calculated frequencies, using the calculated frequencies relatively close to the experimental frequencies. After this calculation a scaling factor of 0.9730 was used to generate the theoretical Raman frequencies. When the BP86/6-31G basis set was utilized in the calculations excellent agreement was obtained between the experimental and calculated frequencies. As a result a scaling factor was not employed. The small percentage difference of 3.37 between the calculated and experimental values significantly increased the accuracy of the vibrational mode assignments. The observed (FT-Raman) and calculated (BP86/6-31G (d, p)) spectra of DDNQ are shown in Figs. 2–4 respectively. A detailed assignment of the vibrational modes of DDNQ using BP86/6-31G (d, p), B3LYP/6-31G (d) and PED is presented in Table 1.

Fig. 2 shows the observed FT-IR spectrum of DDNQ. The most intense frequencies in the FT-IR spectrum are observed at 773, 823, 933, 1137, 1209, 1557, 1601, 1642 and 1668 cm^{-1}. Other relatively weak frequencies are observed at 871, 1274, 1343 and 1580 cm^{-1}.Fig. 1

Fig. 3 shows the experimental Raman spectrum of DDNQ at 1064 nm laser excitation. The intense frequencies in the Raman spectrum are observed at 467, 932, 1180, 1276, 1339, 1581 and 1659 cm^{-1}. Other relatively weak frequencies are observed at 397, 563, 771, 1043, 1161 and 1458 cm^{-1}. The corresponding intense frequencies in the simulated Raman spectrum (Fig. 4) are observed at 457, 929, 1165, 1349, 1567, 1666 cm^{-1}.

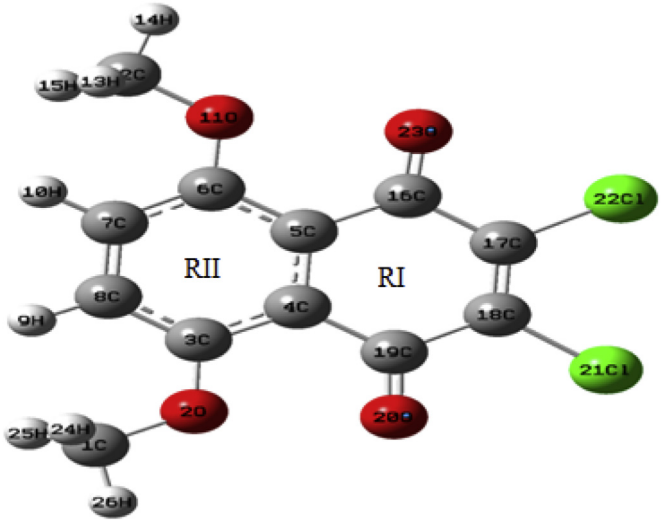

Fig. 1. The molecular structure of 2,3-dichloro-5,8-dimethoxy-1,4-naphthoquinone (DDNQ).

3.1.1. Region above 1800 cm^{-1}

For aromatic molecules, the C–H stretching is observed in the 3050 -3000 cm^{-1}. The 1,4-naphthoquinone molecule shows C–H stretching vibrations at 3076 and 3020 cm^{-1} [22,23]. The Raman spectrum of DDNQ shows four bands at 2842, 2937, 3020 and 3093 cm^{-1} corresponding to the bands observed at 2938, 2939, 3088 and 3157 cm^{-1} in the simulated Raman spectra of DDNQ. The bands at 3025 and 3093 cm^{-1} are assigned to the C–H stretching vibration of the naphthoquinone ring [21,22]. Vibration modes from the methyl group are found in the 2800–3000 cm^{-1} frequency region [24,25]. The bands at 2842 and 2937 cm^{-1} are assigned to the C–H stretching vibration in the methoxy group.

3.1.2. Region 1800–1000 cm^{-1}

The C=O, C=C, ring stretching and C–H bending modes are observed in this spectral window. Strong bands are observed at 1043, 1180, 1276, 1339, 1581 and 1659 cm^{-1} with the bands at 1180 and 1581 cm^{-1} possessing shoulders at 1161 and 1558 cm^{-1} respectively. Other weak bands are observed at 1135, 1401 and 1458 cm^{-1}. The two most intense bands in the Raman spectrum of DDNQ are observed at 1659 and 1581 cm^{-1}. The band observed at 1659 cm^{-1} corresponds to the band at 1660 cm^{-1} in the simulated spectra (Fig. 4 and Table 1). Tabrizi reported a band at 1650 cm^{-1} in the Raman spectrum of 5,8-dihydroxy-1,4-naphthoquinone and assigned that band to the symmetric C=O stretching strongly coupled to the C–C stretching of the rings [21]. Based on this finding, the band at 1659 cm^{-1} is assigned to the C=O symmetric stretching mode which is strongly coupled to a C–C stretching mode. This assignment is consistent with literature data, except that for DDNQ the C=O band is observed at a slightly higher frequency than the frequency reported by Tabrizi [21]. This slight difference in the frequency is due to the electron withdrawing effect of the chloro group in position 2 and 3 of the naphthoquinone ring on the C=O in DDNQ.

The bands in the 1577–1621 cm^{-1} spectral region are assigned to C=C stretching and benzene ring C–C stretching vibrations. Tabrizi reported a band at 1596 cm^{-1} in the Raman spectrum of 5,8-dihydroxy-1, 4-naphthoquinone and assigned it to the C–C stretching coupled with the C–H deformation [21,26]. For DDNQ, the band at 1581 cm^{-1} is assigned to this vibration.

The PED calculation shows that the vibrational modes observed at 1276, 1339, 1401 and 1458 cm^{-1} are predominantly ring C–C/O–C stretching and O–C–H bending modes. The weak broad band that is observed at 1458 cm^{-1} is assigned to 38% O–CH_3 and 31% CH_3 bending vibration based on the work of Tabrizi who also observed a band at 1455 cm^{-1} in the Raman spectrum of 5,8-dihydroxy-1,4-naphthoquinone [21,27]. The band at 1339 cm^{-1} is assigned to 76% ring R_{II} stretch. This assignment is supported by the work of Pecile who observed a band at 1330 cm^{-1} in the Raman spectrum of naphthoquinone and assigned it to a ring stretching vibration [28,29]. The strong band at 1276 cm^{-1} is assigned to 14% C–O stretching and 60% O–CH_3 bending. This assignment is supported by the work of Tabrizi who reported a band at 1260 cm^{-1} in the Raman spectrum of 5,8-dihydroxy-1,4-naphthoquinone and assigned it to the C–O stretching coupled to C–C stretching and C–H in plane bending. Also, Grafton and Wheeler observed a band at 1260 cm^{-1} at in the Raman spectrum of naphthoquinone, and assigned it to the C–H in-plane bending [21,22].

Other bands observed in the spectrum at 1180, 1135 and

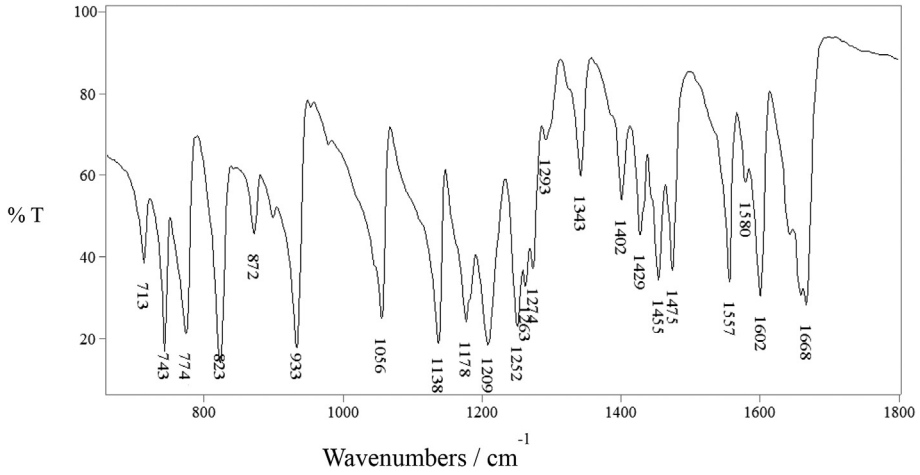

Fig. 2. The FT-IR spectrum of 2,3-dichloro-5,8-dimethoxy-1,4-naphthoquinone.

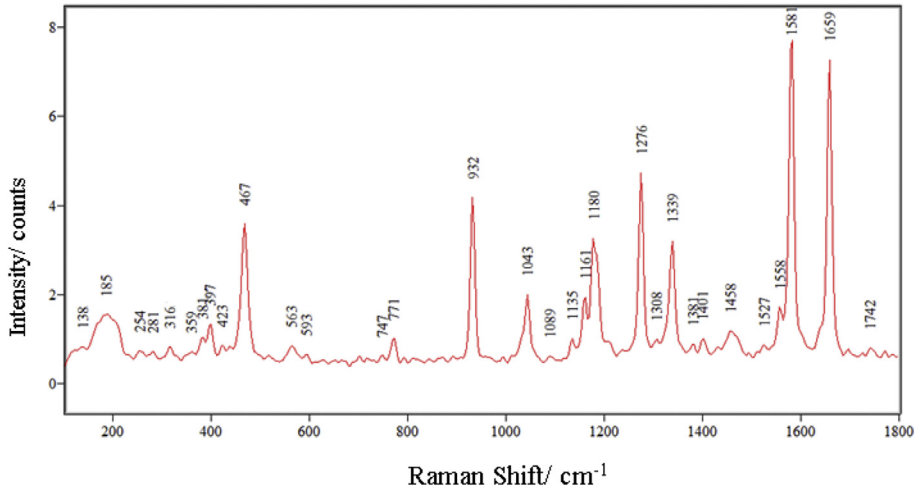

Fig. 3. Raman spectrum of 2,3-dichloro-5,8-dimethoxy-1,4-naphthoquinone.

1043 cm^{-1} are assigned primarily to O–C–H bending coupled to C–C stretching and C–C=O bending vibrations. The band at 1180 cm^{-1} is assigned to C–C stretching coupled to C–C=O bending vibration. For naphthoquinone and its derivatives, the methyl wagging modes which appear in the 1180–1160 cm^{-1} spectral regions, arise primarily from the coupling of the out-of-plane and in-plane bending modes. For DDNQ, the bending/wagging modes of the OCH_3 group were observed at 1161 and 1135 cm^{-1}. The C–O stretching vibrations involving the oxygen atom of the methoxy group and carbon atom of the methoxy and naphthoquinone ring were assigned with the support of the PED calculation. The band at 1043 cm^{-1} is assigned to 46% C–O stretching mode coupled to 16% C–C stretching mode based on the PED calculation [27,30,31].

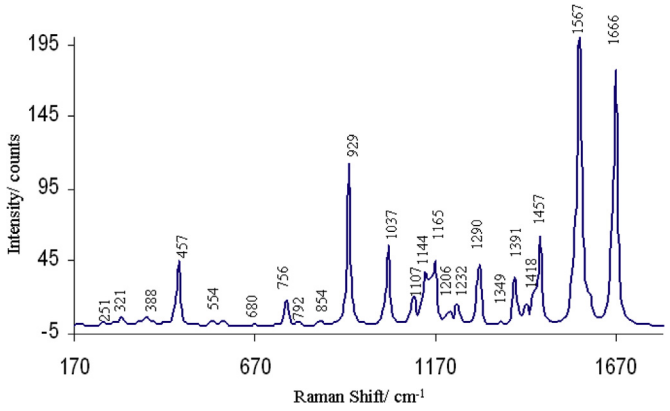

Fig. 4. The simulated Raman spectrum of 2,3-dichloro-5,8-dimethoxy-1,4-naphthoquinone.

3.1.3. *The spectral region below 1000 cm^{-1}*

The C–C–C–C torsion, C–Cl stretching, and C–C–C/O–C–H/C–C–H bending modes are observed in this spectral region. In the Raman spectrum of DDNQ two strong bands are observed at 468 and 932 cm^{-1} and other relatively weaker bands at 316, 397, 563, 771 cm^{-1}. The strong Raman band at 932 cm^{-1} is assigned to the C–C/C–O/C–Cl stretching coupled to R_{II} bending. This assignment is supported by the work of Tabrizi who observed a band at 945 cm^{-1} in the Raman spectrum of 5,8-dihydro-1,4-naphthoquinone and assigned the band to the C–C–C bending vibration coupled to C=O stretching mode [21]. This assignment is also supported by the work of Govindarajan who observed a band at 923 cm^{-1} in the Raman spectra of 1-methoxynaphthalene and assigned the band to the C–C–C bending vibration [25].

Table 1
Band assignments of the vibrational modes of DDNQ.

Number		B3LYP			BP86		Experimental		
	Symmetry	6-31G (d)	6-31G (d) scaled	Raman Activity	6-31G (d, p)	Raman activity	FT-Raman	% Difference	Assignment (PED>5%)
1	B2	3231	3144	65	3143	73	3093	1.61	√C–H (98)
2	A1	3170	3084	228	3088	243	3025	2.08	√C–H_3 (88)
3	B2	3170	3084	1	3088	0			√C–H_3 (88)
4	A1	3029	2948	242	2939	302	2937	0.06	√C–H_3 (92)
5	B2	3028	2947	26	2938	49	2842	3.37	√C–H_3 (92)
6	A1	1751	1703	256	1666	242	1659	0.42	√C=O (76) + β R_I (6)
7	A1	1637	1593	265	1567	269	1581	0.88	√C=C (63)
8	B2	1608	1565	25	1549	16	1558	0.57	√R_{II} (60) + β R_{II} (14)
9	A2	1526	1484	46	1457	48	1458	0.06	βO-CH_3 (38) + β CH_3 (31)
10	B2	1482	1442	12	1418	14	1401	1.21	βO-CH3 (94)
11	A1	1442	1403	10	1391	34	1381	0.65	√C–C(35) +βO-CH_3 (38)
12	A1	1362	1325	15	1349	2	1339	0.74	√R_{II} (76)
13	A1	1333	1297	88	1290	43	1276	1.09	√C–O (14) +βO-CH_3(60)
14	B2	1278	1243	17	1232	17	1241	0.72	√R_I (26)+ βR_I (9) + β O–CH (20)
15	A1	1244	1210	23	1206	14	1180	2.2	√C–C/R_I(63) +βC-C=O (14)
16	A1	1215	1182	48	1165	69	1161	0.34	βO-CH (90)
17	A1	1192	1160	18	1144	57	1135	0.79	βO-CH (74)
18	B2	1148	1117	19	1107	24	1091	1.46	√C–C(26) + βR_I/R_{II} (30)
19	A1	1078	1049	44	1037	66	1043	0.57	√C–O (46) + √C–C(16)
20	A1	959	933	102	929	114	932	0.32	√C–C(10) + √C–O(26) + √C–Cl(12) + βR_{II}(12)
21	B2	880	856	6	854	5	869	1.72	√C–Cl(32) + √R_I(13) + βR_I/R_{II}(18)
22	B1	833	810	1	792	2	792	0.12	TR_{II}(24) + ϕCCCO(22) + βC-C-H(48)
23	B2	784	763	2	756	4	771	1.94	βR_{II}(17) + β[C–C=O](34) + β[C–C–Cl](22)
24	A1	570	554	5	554	6	563	1.59	βC-C-O(22) + βO-CH_3 (18) + βR_{II} (11)
25	A1	472	459	46	457	58	467	2.14	βR_I(59) + √C–C (13) + βR_{II} (7)
26	B2	432	420	1	419	1	423	0.94	βR_I(29) + √C–Cl (20) + βC-C=O (14)
27	A1	405	394	2	388	4	397	2.26	βR_{II}(37) + βC-C=O (34)
28	B2	321	313	2	321	1	316	1.26	βO-CH(34) + βR_{II}/R_I(17) + βC-C-Cl(14)
29	B2	260	253	2	251	3	254	1.18	βR_I(43) + βC-C-Cl(14) + √C–C(12) + β R_I (6)
30	A1	190	185	2	185	3	185	1.08	TCCCO(38) + ϕCCCl(24) + β O–CH (16) + TR_{II}(7)

√: Stretching; β: In-plane bending; φ: Out-of-plane bending; T:Torsion.

The C–Cl stretching frequency is generally observed in the 800–600 cm^{-1} spectral region and is dependent on the conformation of the compound [30]. The weak band at 869 cm^{-1} is assigned to C–Cl stretching while the other weak band at 771 cm^{-1} is assigned to C–C=O bending coupled to R_{II} and C–C–Cl bending, and the band at 563 cm^{-1} is assigned to C–C–O/O–CH_3/R_{II} bending. The strong band at 467 cm^{-1} is assigned to ring bending vibrations. The complete vibrational assignment is shown in Table 1.

3.2. Surface enhanced Raman scattering (SERS) spectrum of 2,3-dichloro-5,8-dimethoxy-1,4-naphthoquinone

Fig. 5 shows the UV–visible absorption spectrum of the gold nano-rods. The peaks at 530 and 760 nm are typical features of gold nano-rods and represent the transversal and longitudinal plasmonic bands [32]. Dynamic light scattering was used to determine the dimensions of the gold nano-rods and the results from these studies indicate that there is good monodispersity of gold nanorod size with dimensions of 43 nm (length) by 16 nm (width).

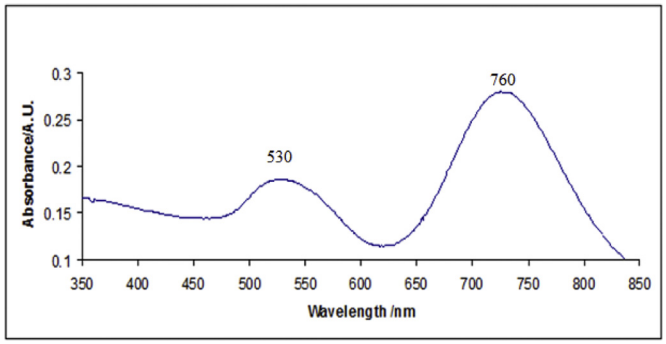

Fig. 5. The UV–visible spectrum of gold nano-rods.

The SEM image of the gold nano-rods deposited on a silicon wafer substrate is shown in Fig. 6.

3.2.1. Adsorption of DDNQ

DDNQ has a number of potential adsorption sites for possible interactions with metal surfaces: the π electrons of the naphthoquinone ring, the lone pair of electrons on the oxygen atoms, and the chlorine atoms. Based on changes in relative band intensities between the solution and the SERS spectrum of DDNQ adsorbed on gold nano-rods, the preferred molecular adsorption site of DDNQ on gold surface along with its orientation can be determined. SERS has been used to study the adsorption mechanism of molecule adsorbed onto the surface of coinage metals [5,6]. The adsorbate SERS spectrum is analyzed based on shifts in the SERS frequencies and relative enhancing or weakening of the intensity of the SERS bands compared to their solution counterparts [12,33–35]. For this study Gold nano-rods were selected because they are an attractive alternative to spherical metallic nanoparticles for exploring a wide range of surface plasmon enhanced sensing application. It is possible to achieve a strong optical extinction at targeted wavelengths by adjusting the rod aspect ratio [36].

Fig. 7 shows the Raman spectrum of gold nano-rods deposited on a silicon wafer (black spectrum) and the SERS spectrum of DDNQ adsorbed onto the gold nano-rods (red spectrum). One limitation to the use of gold nanorods, as prepared by the above described method, for SERS has been the presence of bands due to residual CTAB which remains attached to the nanorods. The characteristic CTAB Raman bands are normally observed at 455, 763, 1061, 1127, 1295 and 1460 cm^{-1}. An examination of the Raman spectrum of the nanorods, after deposition, indicates the absence of bands at these frequencies. Only the Si band at 517 cm^{-1} is observed in the

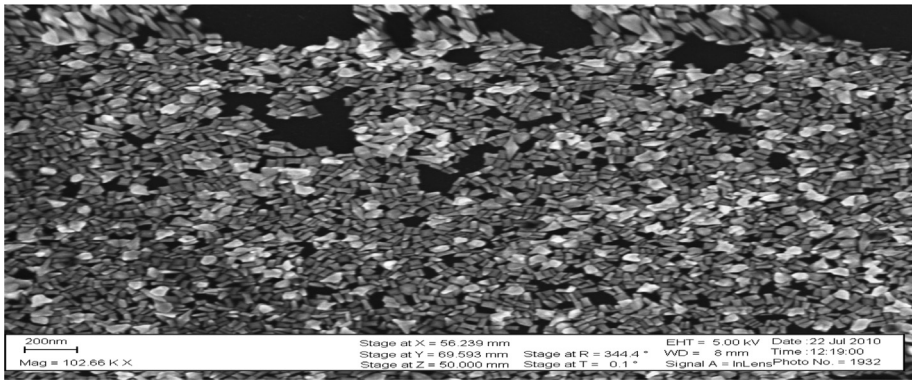

Fig. 6. The SEM image of gold nano-rods chemically deposited on silicon wafer.

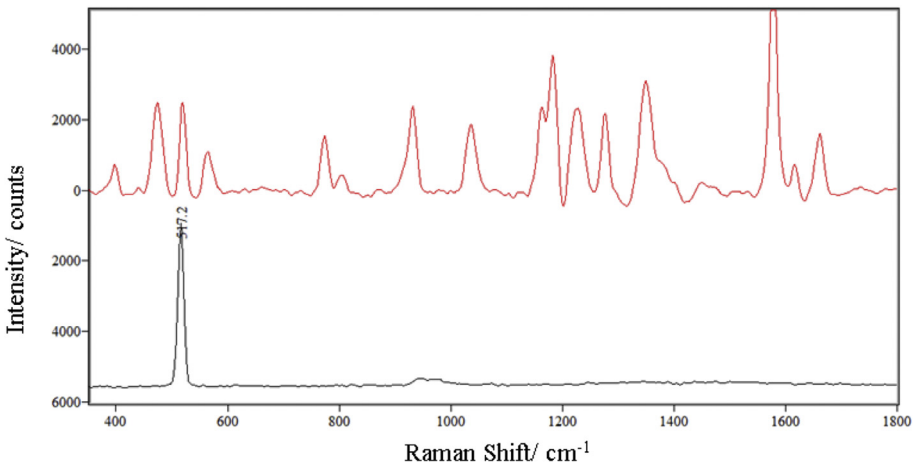

Fig. 7. SERS spectra of gold nano-rods on silicon wafer (black line) and DDNQ adsorbed on the gold nano-rods (Red line). (For interpretation of the references to color in this figure legend, the reader is referred to the web version of this article.)

spectrum (Fig. 6). When DDNQ is adsorbed onto the SERS active gold nano-rods, bands characteristic of the Raman active modes of DDNQ were observed with an excellent signal to noise ratio. The Raman spectrum of DDNQ from a solution having the same concentration as that used in the SERS studies is shown in Fig. 7.

Fig. 8 shows the solution Raman (0.348 M) and SERS spectra of DDNQ. A comparison of the SERS and Raman spectra shows a marked difference in both band frequencies and relative intensities.

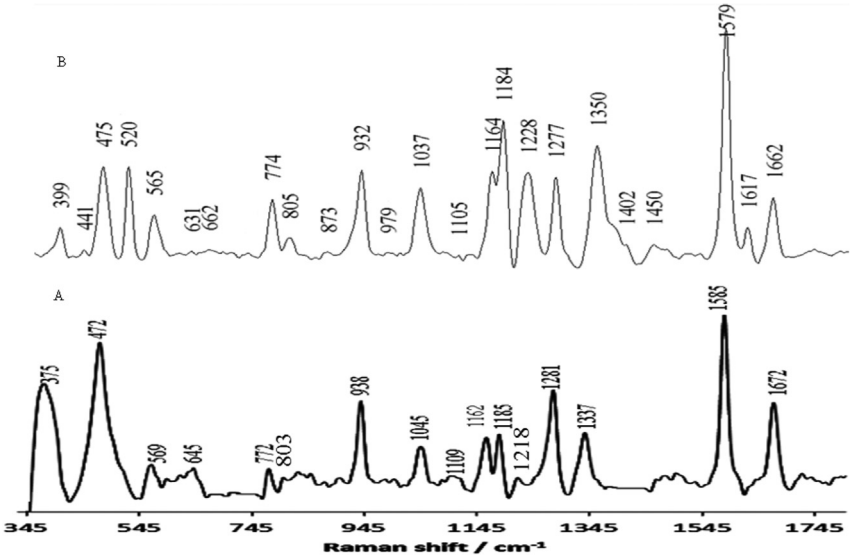

Fig. 8. (A) Solution Raman and (B) SERS spectra of DDNQ adsorbed on the gold nano-rods.

The SERS spectrum is dominated by strong bands at 1579, 1350, 1277, 1228, 1184, 1037 and 932 cm^{-1} while the bands observed at 1662, 1579, 1350, 1037 and 399 cm^{-1} in the SERS spectrum are shifted compare to their solution Raman counterparts. The solution Raman band at 1672 cm^{-1} was down shifted by 10 wavenumbers in the SERS spectrum to 1662 cm^{-1}, while the solution Raman band at 1337 cm^{-1} was up shifted by 13 wavenumbers in the SERS spectrum to 1350 cm^{-1}. The SERS band at 1037 cm^{-1} is down shifted by 8 wavenumbers when compare to its solution counterpart observed at 1045 cm^{-1}. The Raman band at 1585 cm^{-1} was down shifted by 6 wavenumbers in the SERS spectrum to 1579 cm^{-1}. The band at 1585 cm^{-1} is strong in both the Raman and SERS spectra and has been assigned to C=C stretching vibration of the naphthoquinone ring [21,22,26].

Ramakrishnan reported SERS of 1-aminoanthraquinone (AAQ) on Ag colloids and observed that the C=O band was shifted to a lower frequency relative to its solution counterpart. This led the authors to conclude that AAQ was adsorbed on the Ag surface via C=O group [37,38]. Also, Jurasekova reported the SERS of quercetin adsorbed on Ag colloid and observed that the C=O band observed at 1655 cm^{-1} in the solution spectrum was down shifted to 1640 cm^{-1} in the SERS. The C=O band in these SERS spectra also exhibited a reduction in intensity relative to their solution counterparts. Based on these observations the authors concluded that the interaction between the quercetin and the Ag surface involved the C=O substituent 38. In the SERS spectrum of DDNQ, the band observed at 1662 cm^{-1} was assigned to C=O stretching vibration, is downshifted by 10 wavenumbers relative and its intensity is reduced relative to its solution counterpart. The observed shift in frequency and the reduced intensity suggests that DDNQ is adsorbed on the surface of the gold nano-rods via the C=O group.

3.2.2. Orientation of DDNQ

SERS relative enhancement factors (SEF) can be utilized to deduce the orientation of molecules adsorbed on SERS active surfaces. The solution Raman and SERS intensities of DDNQ were normalized and the normalized intensities are shown in Table 2. Based on relative enhancement factors and the use of surface selection rules developed by Creighton, an orientation of DDNQ adsorbed on Au nano-rods is proposed.

The adsorbate orientation can in principle be obtained from surface vibrational band intensities using the surface selection rule proposed by Moskovits and Creighton for C_{2v} aromatic molecules [39,40]. According to the surface selection rules, the vibration modes possessing polarizability tensors in the direction of the surface normal should experience the greatest intensity enhancement in the SERS spectrum, namely vibrational modes corresponding to α_{zz}, where z is along the surface normal. Vibrations derived from α_{xz} and α_{yz} should be the next most intense modes and those corresponding to α_{xx}, α_{yy}, α_{xy} polarization elements should be the least enhanced [41,39]. The most enhanced bands are related to the modes containing the components of polarizability tensor perpendicular to the surface. An examination of the Table 2 shows that ring stretching modes at 1037, 1184, 1228 and 1350 cm^{-1} in the SERS spectrum of DDNQ exhibit large enhancement factor.

Based on the relationship between relative enhancement factor and mode symmetry Creighton proposed a relationship between adsorbate orientation and relative band enhancement factors. For a flat orientation the surface selection rules predict that the SEF for the A2 modes should be enhanced relative to the B2 modes and that the reverse is true for a molecule which adopts a perpendicular orientation [42]. Inspection of the SEF values for DDNQ adsorbed onto Au nano-rods show them to be consistent with the selection rule prediction of the molecule being oriented perpendicular to the metal surface.

The ratio of the intensity of the ring modes to those of the C=O stretching mode in the Raman spectrum, compared to the SERS spectrum can be utilized to determine the orientation of the adsorbed molecule. Nishiyama used the ratio of the intensity of the aromatic ring mode to that of the C=O stretching mode of anthraquinone derivatives, to determine the orientation of the molecule on silver surface. When the ratio of the intensities of ring modes to that of the C=O stretching band in the SERS was enhanced compared with that of the solution Raman bands, it suggests that the molecular plane has a relatively perpendicular orientation compared to the Ag surface. It also suggests that the ring mode has a vertical component to the surface, which is enhanced in the SERS spectrum [43]. For DDNQ, the intensities of the ring modes are strongly enhanced in the SERS spectrum relative to that of the C=O. The enhancement factor is shown in Table 2. The ratio of the intensity of the C–C stretching modes to that of the C=O stretching mode in the SERS ($I_{ring\ (1350)}/I_{C=O\ (1662)} = 1.88$; $I_{ring\ (1037)}/I_{C=O\ (1662)} = 1.16$) was enhanced compared with that of the Raman ($I_{ring\ (1340)}/I_{C=O\ (1662)} = 0.62$; $I_{ring\ (1043)}/I_{C=O\ (1662)} = 0.42$). The result suggests that DDNQ is adsorbed with its molecular plane that is relatively perpendicular to the gold nano-surfaces. The proposed orientation of DDNQ is shown in Fig. 9.

Table 2
The normalized relative intensities and the relative enhancement factor for DDNQ in solution compared with adsorbed DDNQ (SERS).

Symmetry modes	Raman	Au nano-rods-SERS	REF
	cm-1	cm-1	
A1	1672 (0.47)	1662 (0.25)	0.53
A1	1585 (1)	1579 (1)	1
A2	1481 (0.02)	1450 (0.06)	3
A1	1337 (0.29)	1350 (0.47)	1.62
A1	1281 (0.55)	1277 (0.33)	0.6
B2	1218 (0.01)	1228 (0.35)	35
A1	1185 (0.28)	1184 (0.59)	2.11
A1	1162 (0.26)	1164 (0.36)	1.38
A1	1109 (0.01)	1130 (0.01)	0.8
A1	1045 (0.2)	1037 (0.29)	1.45
A1	939 (0.48)	933 (0.37)	0.77
B2	854 (0.01)	873 (0.29)	29
A1	775 (0.07)	775 (0.24)	3.43
A1	567 (0.09)	565 (0.17)	1.89
A1	475 (0.83)	475 (0.38)	0.46
A1	375 (0.58)	399 (0.11)	0.19

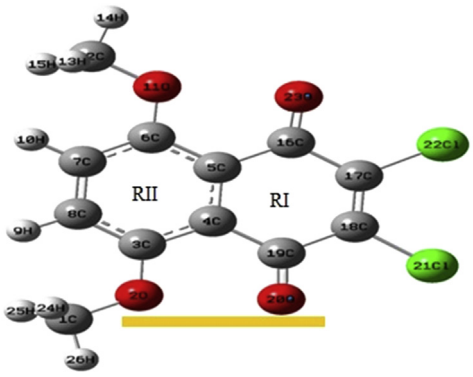

Fig. 9. Proposed Orientation of 2,3-dichloro-5,8-dimethoxy-1,4-naphthoquinone on the gold nano-rods.

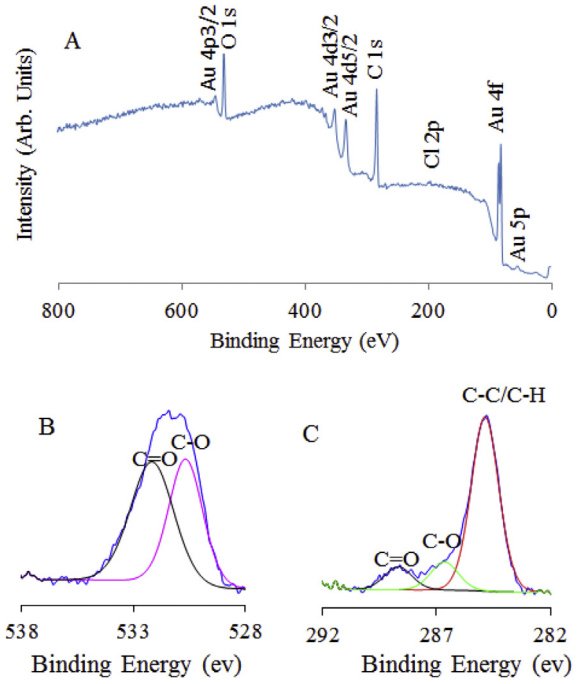

Fig. 10. XPS spectrum of DDNQ adsorbed onto the gold surface.

adsorbed onto the Au surface.

The relative oxygen and carbon content of the Au surface before and after DDNQ adsorption shows that the oxygen and carbon content increased when DDNQ was adsorbed onto the surface. Fig. 11a shows the plot of O/Au ratio versus the take-off angles, while Fig. 11b shows the plot of C/Au ratio versus the take-off angles. The SAMs of DDNQ on the Au surface shows higher O/Au or C/Au ratio than Au surface showing a thicker layer of DDNQ present due to adsorption of DDNQ on the Au surface. The relative content of carbon and oxygen on the Au surface before and after adsorbing DDNQ and the presence of chlorine after DDNQ adsorption establish that DDNQ was successfully adsorbed on the Au surface.

4. Conclusions

Raman spectroscopy, SERS, XPS and DFT methods have been used to investigate the adsorption and orientation of SAMs of 2, 3-dichloro-5, 8-dimethoxy-1, 4-naphthoquinone (DDNQ) on gold nano-rods. The Raman band assignment of the DDNQ molecule was made on the basis of comparison with literature values, DFT calculations, and PED calculations. From the SERS spectrum, the C=O stretching vibrational mode was red shifted by 10 wavenumbers relative to its solution counterpart indicating that DDNQ is adsorbed onto the gold nano-rods via the C=O group. The SERS intensities of the ring modes, observed at 1350, 1228, 1037 cm^{-1}, exhibited large enhancement factors relative to their solution

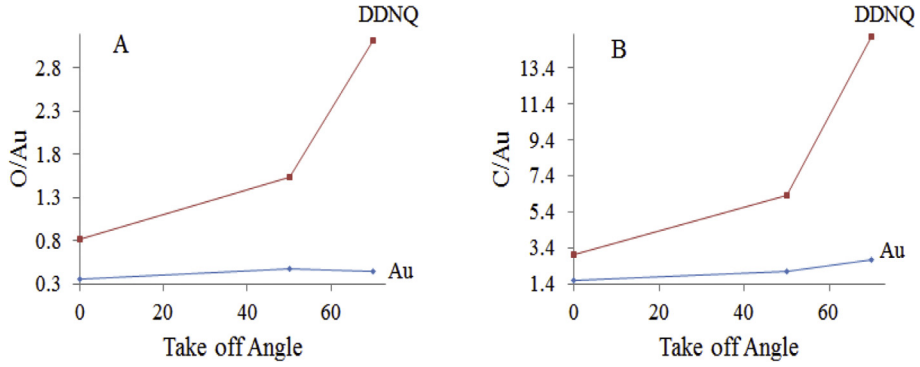

Fig. 11. A plot of (a) the O/Au ratio versus the take-off angle and (b) the C/Au ratio versus the take-off angle before and after adsorption of DDNQ onto the Au surface.

3.3. *XPS study of the adsorption of DDNQ on gold surface*

DDNQ was self-assembled onto a Au surface and X-ray photoelectron spectroscopy (XPS) was utilized to study the adsorption of DDNQ to the Au surface [40]. The resulting XPS spectrum of DDNQ on a Au surface, Fig. 10a, shows the C 1s, O 1s and Cl 2p peaks.

The high resolution spectrum of the C 1s region is shown in Fig. 10c. The C 1s spectrum was deconvoluted into three individual component peaks. The peak binding energies at 286.7, 288.7 and 284.8 eV can be assigned to the carbon atom in the form of C—O (ether), C=O (quinone) and C—C/C—H respectively [44,45]. As shown in Fig. 10c for the DDNQ C 1s binding energy, the observation of the growth of the C 1s peak at 284.8 eV confirms that DDNQ was adsorbed onto the Au surface. The appearance of the C 1s C=O peak at 288.7 eV indicates the present of a carbonyl group on the Au surface [44]. In addition, it can be observed in Fig. 10b that the deconvolution of the O 1s spectrum produces two peaks with binding energy at 530.7 and 532.2 eV which are assigned to C=O (quinone) and C—O (ether) respectively [46]. The observation of the growth of the O 1s peak at 530.7 eV confirms that DDNQ was counterparts. On the basis of SERS selection rules, it was concluded that the adsorbed DDNQ has a perpendicular orientation on the surface of the gold nano-rods. The XPS data showed the growth of the C 1s and O 1s characteristic peaks confirming that DDNQ was adsorbed onto the Au surface.

Acknowledgments

This work was supported by the STC Center for Integrated Quantum Materials, NSF Grant No. DMR-1231319.

References

[1] G.A. Silva, G.A. Neurocience Nanotechnology, progress, opportunities and challenges, Nat. Rev. Neurosci. 7 (2006) 65–74.
[2] J.P. Sumner, J.W. Aylott, E. Monson, R. Kopelman, Analyst 127 (2002) 11–16.
[3] S. Bhattacharyya, S. Prashanthi, P.R. Bangal, A. Patra, J. Phys. Chem. C 117 (2013) 26750–26759.
[4] C. Ding, A. Zhu, Y. Tian, Acc. Chem. Res. 47 (2014) 20–30.
[5] J. Gao, H. Gu, B. Xu, Acc. Chem. Res. 42 (2009) 1097.
[6] C.K. Kim, P. Ghosh, C. Pagliuca, Z. Zhu, S. Menichetti, V.M. Rotello, J. Am. Chem. Soc. 131 (2009) 1360.
[7] D.C. Hone, P.I. Walker, R. Evans-Gowing, S. FitzGerald, A. Beeby, I. Chambrier,

M.J. Cook, D.A. Russell, Langmuir 18 (2002) 2985.
[8] J.R. Hwu, Y.S. Lin, T. Josephrajan, M. Hsu, F. Cheng, C. Yeh, W. Su, D. Shieh, J. Am. Chem. Soc. 131 (2009) 66.
[9] D.C. Hone, P.I. Walker, R. Evans-Gowing, S. Fitzgerald, A. Beeby, I. Chambrier, M.J. Cook, D.A. Russell, Langmuir 18 (2002) 2985.
[10] Y. Cheng, J.D. Meyers, A.-M. Broome, M.E. Kenney, J.P. Basilion, C. Burda, J. Am. Chem. Soc. 113 (2011) 2583–2591.
[11] E. C. Dreaden, S. C. Mwakwari, Q. H. Sodji, A. K. Oyelere, M. A. El-Sayed.
[12] S. Zong, Z. Wang, H. Chen, J. Yang, Y. Cui, Anal. Chem. 85 (2013) 2223–2230.
[13] Y. Cheng, A.C. Samia, J.D. Meyers, I. Panagopoulos, B.W. Fei, C. Burda, J. Am. Chem. Soc. 130 (2008) 10643.
[14] R.L. Copeland, J.R. Das, O. Bakare, N.M. Enwerem, S. Berhe, K. Hillaire, D. White, Anticancer Res. 27 (2007) 1537–1546.
[15] L.-J. Huang, F.-C. Chang, K.-H. Lee, J.-P. Wang, C.-M. Teng, S.-C. Kuo, Med. Chem. 6 (1998) 2261–2269.
[16] T.K. Sau, C.J. Murphy, Langmuir 20 (2004) 6414.
[17] O.M. Primera-Pedrozo, Synthesis Surface Modification of Metallic Nanoparticles: Sensitivity, Influence of Shape, Concentration and Excitation Wavelength on Chemical Detection by SERS, 2010. Thesis.
[18] Y.K. Park, S.H. Yoo, S. Park, Langmuir 23 (23) (2007) 10505–10510.
[19] W. Wang, B. Gu, J. Phys. Chem. B 109 (2005) 22175–22180.
[20] J.M.L. Martin, C. Van Alsenoy, Gar2ped, University of Antwerp, 1995.
[21] M.Z. Tabrizi, S.F. Tayyari, F. Tayyari, M. Behforouz, Spectrochim. Acta Part A 60 (2004) 111–120.
[22] A.K. Grafton, R.A. Wheeler, J. Phys. Chem. A 101 (1997) 7154–7166.
[23] S.N. Singh, R.S. Singh, Spectrochim. Acta 24A (1968) 1591–1597.
[24] S.J. Bunce, H.G. Edwards, A.F. Johnson, I.R. Lewis, P.H. Turner, Spectrochim. Acta 49 (1993) 775–783.
[25] M. Govindarajan, K. Ganasan, S. Periandy, M. Karabacak, Spectrochim. Acta Part A 79 (2011) 646–653.
[26] G. Balakrishnan, P. Mohandas, S. Umapathy, J. Phys. Chem. 100 (1996) 16472–16478.
[27] A. Bulovas, N. Dirvianskyte, Z. Talaikyte, G. Niaura, S. Valentukonyte, E. Butkus, V. Razumas, J. Electroanaly. Chem. 591 (2006) 175–188.
[28] C. Pecile, B. Lunelli, V. Busetti, J. Chem. Soc. A 5 (1970) 690–697.
[29] A. Girlando, D. Ragazzon, C. Pecile, Spectrochim. Acta 36A (1980) 1053–1058.
[30] M. Kazemekaite, A. Bulovas, Z. Talaikyte, E. Butkus, V. Railaite, G. Niaura, A. Palaima, V. Razumas, Tetrahedron Lett. 45 (2004) 3551–3555.
[31] G. Fabriciova, J.V. García-Ramos, P. Miskovsky, S. Sanchez-Cortes, Vib. Spectrosc. 30 (2002) 203–212.
[32] C.J. Orendorff, A. Gole, T.K. Sau, C.J. Murphy, Anal. Chem. 77 (2005) 3261–3266.
[33] H.T. Varghese, C.Y. Panicker, D. Philip, J.R. Mannekutla, S.R. Inamdar, Spectrochim. Acta Part A 66 (2007) 959–963.
[34] P. Gao, M.J. Weaver, J. Phys. Chem. 89 (1985) 5040–5046.
[35] Y. Fleger, Y. Mastai, M. Rosenbluh, D.H. Dressler, Surf. Sci. 603 (2009) 788–793.
[36] D. Graham, K. Faulds, Chem. Soc. Rev. 37 (2008) 1042–1051.
[37] V. Ramakrishnan, N. Krishnamurthy, M. Gurunathan, V.J.P. Srivatsavoy, Spectrochim. Acta 46A (1990) 1615–1619.
[38] Z. Jurasekova, A. Torreggiani, M. Tamba, S. Sanchez-Cortes, J.V. Garcia-Ramos, J. Mol. Struct. 918 (2009) 129–137.
[39] M. Moskovits, J.S. Suh, J. Phys. Chem. 88 (1984) 5526–5530.
[40] J.A. Creighton, Surf. Sci. 124 (1983) 209–219.
[41] X. Gao, J.P. Davies, M.J. Weaver, J. Phys. Chem. 94 (1990) 6858–6864.
[42] B. Nikoobakht, M.A. El-Sayed, J. Phys. Chem. A 107 (2003) 3372–3378.
[43] D. Graham, K. Faulds, Chem. Soc. Rev. 37 (2008) 1042–1051.
[44] K. Nishiyama, S.-I. Tahara, Y. Uchida, S. Tanoue, I. Taniguchi, J. Electroanal. Chem. 478 (1999) 83–91.
[45] Y. Fleger, Y. Mastai, M. Rosenbluh, D.H. Dressler, Surf. Sci. 603 (2009) 788–793.
[46] S.-F. Lim, Y.-M. Zheng, S.-W. Zou, J.P. Chen, Environ. Sci. Technol. 42 (2008) 2551–2556.